PERGAMON

International Journal of Solids and Structures 37 (2000) 7547–7562

INTERNATIONAL JOURNAL OF SOLIDS and STRUCTURES

www.elsevier.com/locate/ijsolstr

The compressive viscoplastic response of an A359/SiC_p metal–matrix composite and of the A359 aluminum alloy matrix

Y. Li [a], K.T. Ramesh [a,*], E.S.C. Chin [b]

[a] *Laboratory for Impact Dynamics and Rheology, Department of Mechanical Engineering, The Johns Hopkins University, 122 Latrobe Hall, 3400 N. Charles Street, Baltimore, MD 21218-2686, USA*

[b] *Weapons and Materials Research Directorate, Army Research Laboratory, Aberdeen Proving Ground, MD 21005, USA*

Received 21 January 1999

Abstract

The mechanical behaviors of an A359/SiC_p metal–matrix composite and of the corresponding A359 cast aluminum alloy have been measured in compression over a wide range of strain rates (10^{-4}–10^5 s^{-1}) using several different experimental techniques: servohydraulic testing, the compression Kolsky bar, and pressure–shear plate impact. Both the A359 matrix alloy and the A359/SiC_p composite show rate dependence of the flow stress in compression, with rate dependences that increase with increasing strain rate. The unreinforced A359 alloy shows strain hardening that is essentially independent of the strain rate, and similar in most respects to the behavior of wrought aluminum alloys such as 6061. The A359/SiC_p composite shows rate dependence similar to that of the unreinforced alloy, but also shows significantly less strain hardening than does the matrix alloy. This reduction in strain hardening appears to be a result of progressive particle fracture during these compressive deformations. Using the experimental data on the unreinforced A359 aluminum alloy as the input data for the matrix behavior, and accounting for particle shape and aspect ratio, an analytical model developed recently by the authors is used to estimate the mechanical response of the composite over the whole range of strain rates. The model is able to capture the rate dependence of the flow stress of the composite, and is able to provide a reasonable estimate of the flow stress of the composite material at small strains. However, because the model does not incorporate the particle damage that occurs in the composite, it is unable to predict the changed overall strain hardening of the composite material.

Keywords: Matrix composite; Aluminum alloy; Viscoplastic response

1. Introduction and background

Particle-reinforced metal–matrix composites (MMCs) exhibit a significant improvement in mechanical performance over monolithic alloys in many structural applications. Some specific advantages include high specific modulus, high specific strength and high wear resistance. Particle-reinforced MMCs are also relatively easily manufactured (in comparison with fiber-reinforced MMCs), and so have the potential for use

* Corresponding author. Tel.: +1-410-516-7735; fax: +1-410-516-7254.
E-mail address: ramesh@jhu.edu (K.T. Ramesh).

0020-7683/00/$ - see front matter
PII: S0020-7683(99)00304-2

within high-volume commercial products (one recent application is within automobile brake rotors). A specific application of substantial scientific interest consists of functionally graded metal–ceramic composites in which the ceramic particle volume fraction is graded (Mortensen and Suresh, 1995; Suresh and Mortensen, 1997). The current article focuses on the high-strain-rate mechanical properties of ceramic particle-reinforced MMCs. Applications in which the dynamic response of particle-reinforced MMCs is important include aerospace structures subjected to missile and bird impacts, and personnel armor and vehicle armor in defence applications. Functionally graded MMCs designed for optimal performance are of interest in a number of these applications.

The low-rate mechanical properties and failure mechanisms of particle- and whisker-reinforced MMCs have been well characterized over the last decade. A number of theoretical and numerical investigations have been performed to predict the stiffness and the strength of the composite, given the mechanical properties of the matrix and reinforcement phases (Clegg, 1988; Christman et al., 1989a; Tvergaard, 1990). The effects of material parameters such as reinforcement volume fraction, size, shape, aspect ratio and particle distribution on the plastic deformations and failure mechanisms of MMCs under quasistatic loading have been extensively studied (Christman et al., 1989b). Phenomena arising from the heterogeneity of the material microstructure have also been addressed by a number of workers (Taya and Mori, 1987; Taggart and Bassani, 1991).

The mechanical properties of MMCs under high rates of strain are not as well understood. One reason for this is that the response of MMCs to multi-axial loading can be very complex, and so it is difficult to compare the response of materials tested with different dynamic loading techniques. Much of the high-rate literature on such materials has been reviewed in a previous article by the authors (Li and Ramesh, 1998). Only selected references are discussed here.

Modern investigations of the high-rate constitutive response of MMCs (rather than shock response), include the work of Harding et al. (1987) and Marchand et al. (1988). Articles that consider the dynamic material response in terms of microstructural features include those of Perng et al. (1993a,b), Hong and Gray (1994), Mukai et al. (1995), Yadav et al. (1995), Chichili and Ramesh (1995), Vaidya et al. (1996), Gray et al. (1996) and Guden and Hall (1998). Most of these researchers observed an increased rate sensitivity of the composite vis-à-vis, the matrix metal. Yadav et al. (1995) developed a simple model, which indicated that the effect of strain rate would be strongly dependent on the inclusion volume fraction. This issue was examined more rigorously by Bao and Lin (1996) and Yadav (1996), who developed computationally based models for the stress–strain behavior of MMCs at high strain rates using axisymmetric unit cells and a spherical particle approximation. They found that the effect of strain rate is coupled with the inclusion volume fraction; the strain-rate hardening of the composite may be significantly higher than that of the matrix due to the constraining effect of the inclusions. Li and Ramesh (1998) also studied the effects of particle shape and aspect ratio on the high-strain-rate response of MMCs, and concluded that both variables have a strong influence on the flow stress at high strain rates.

This article presents both experimental and computational investigations of the mechanical behavior of an A359/SiC_p MMC in compression over a very wide range of strain rates. This material system is of interest because it is being considered for use within graded armor structures (the matrix is a cast alloy), and there is currently no data on the high-strain-rate behavior. This work focuses on the constitutive response of the composite; investigations of damage and tensile failure are presented elsewhere.

2. Materials

The materials used in the current study were A359 aluminum alloy and the F3S.20S MMC, which is A359 aluminum alloy reinforced by 20 vol% of SiC particles. The A359 aluminum alloy was supplied by Alcan International Limited in the form of a cast bar with a diameter of 1.5 in. The composition (wt.%) of

the A359 aluminum alloy is as follows: 0.2 Cu, 0.5–0.7 Mg, 0.1 Mn, 8.5–9.5 Si, 0.20 Fe, 0.10 Zn, 0.20 Ti, 0.20 others, with the balance being aluminum. The composite was also supplied by Alcan International Limited in the form of an as-cast bar with a diameter of 1.5 in.

Optical micrographs of the as-cast unreinforced alloy and of the as-cast composite are shown in Fig. 1(a) and (b), respectively. The unreinforced alloy shows the classic dendritic microstructure containing fine silicon particles. The composite shows that the reinforcing silicon carbide particles are generally distributed along the eutectic phase boundaries, and it is apparent that there are facets on the particles, as well as a slight preferred orientation. Vickers microhardness measurements (Table 1) in the unreinforced alloy and in the matrix of the composite (with a load chosen, so that the length of the long diagonal of the indent in the matrix was less than half the distance to the nearest particle) indicate that the yield strength of the matrix material is very similar to that of the unreinforced alloy; yield strengths in Table 1 were estimated from the Vickers microhardness numbers using the traditional 1/3 approximation. This, together with the similarity of the microstructures provides some confidence that the rate-dependent properties of the unreinforced alloy can be assumed to be the properties of the matrix in the composite for the purposes of theoretical and analytical modeling.

Quantitative microscopy was used to determine the statistical characteristics of the reinforcement distribution in the composite. Metallographic specimens were prepared by sectioning the as-cast composite bar along the bar axis and transverse to the bar axis (axial and transverse sections) using a low-speed diamond saw. After the surfaces were polished, either optical micrographs or scanning electron micrographs of five locations on each section were used to measure the particle aspect ratio and particle size. The measured distributions of particle size and particle aspect ratio within the axial and transverse sections are

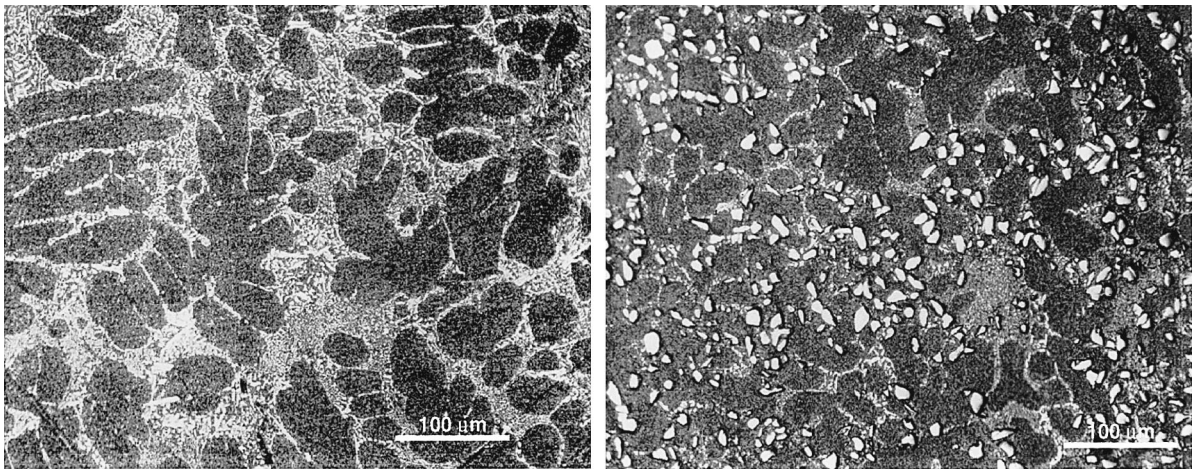

Fig. 1. Optical micrographs of (a) as-received A359 alloy and (b) the as-received F3S.20S MMC (A359 containing 20 vol% SiC particles).

Table 1
Comparison of Vickers microhardness and yield strength of the monolithic alloy and the matrix of the composite materials

Material	Mean diagonal (μm)	Vickers microhardness (kg/mm^2)	Yield strength (MPa)
A359 Al (Alcan)	35.0 ± 0.4	75.6	252
F3S.20S (Alcan)	34.5 ± 0.8	78.0	260

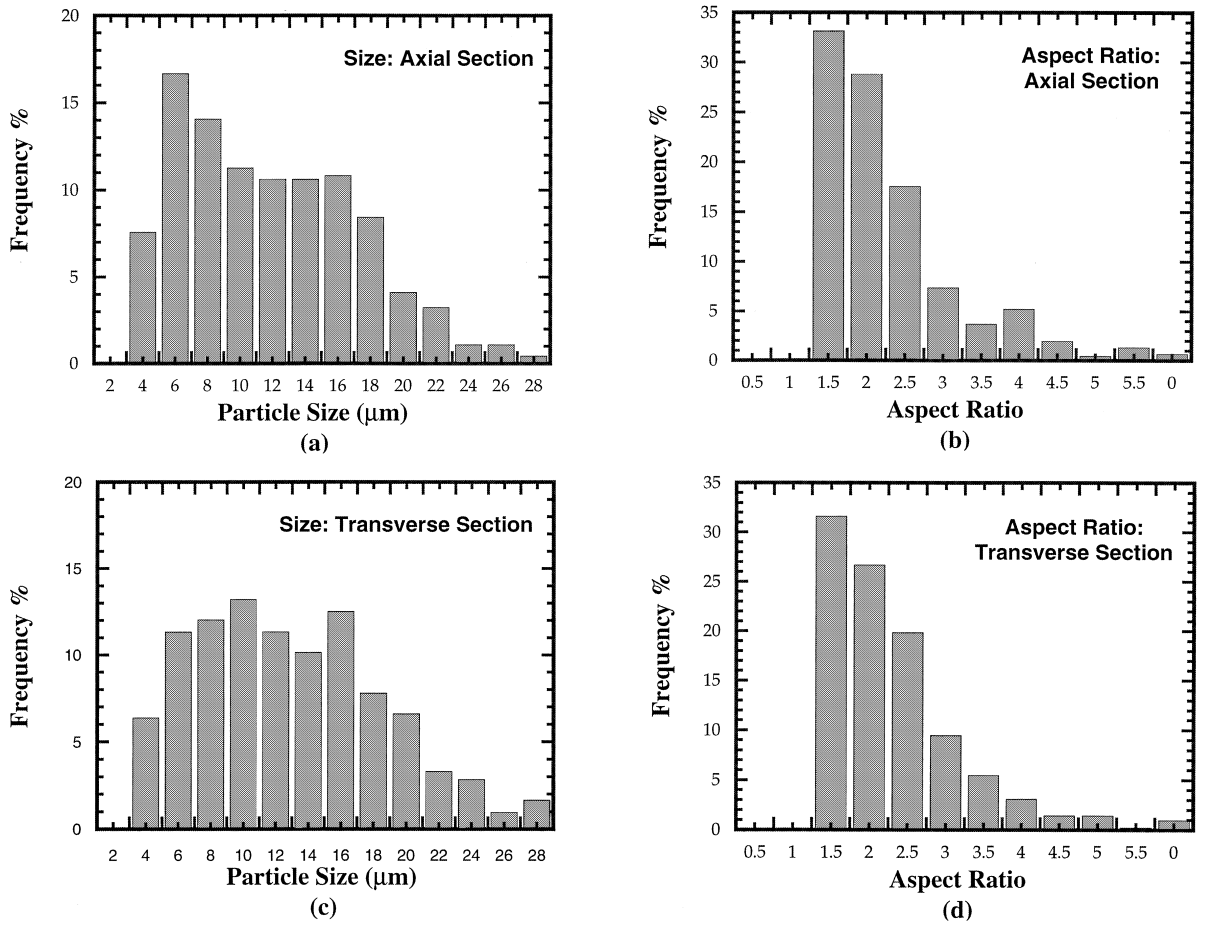

Fig. 2. Distribution of particle size and aspect ratio within the as-received composite: (a) particle size distribution in axial section; (b) aspect ratio distribution in axial section; (c) particle size distribution in transverse section; and (d) aspect ratio distribution in the transverse section.

shown in Fig. 2. It is clear from Fig. 2(c) and (d) that the mean particle size in both axial and transverse sections is around 6–18 μm, but the population of particles with a size smaller than 10 μm is greater in the axial section than in the transverse section (note that these bars are *not* extruded). Most of the particles have aspect ratios around 1.5–2.5 within both axial and transverse sections (Fig. 2(b) and (d)), which suggests that most of the particles are present in the form of small plates. These characteristics of the distributions are slightly different from those measured on a nominally identical composite obtained from Duralcan (Li and Ramesh, 1998), indicating again the variations in structure that can result from variations in processing.

3. Experimental procedures

The rate-dependent mechanical behaviors of both the unreinforced alloy and the MMC were studied (in compression) over a strain-rate range of 10^{-4}–10^{5} s^{-1} using a combination of quasistatic and dynamic testing

techniques: servohydraulic machines at low rates, a compression Kolsky bar at intermediate rates, and high-strain-rate pressure–shear plate impact at extremely high strain rates.

3.1. Quasistatic testing

An MTS servohydraulic testing machine was used to conduct compression experiments in the strain rate range of 10^{-5}–1 s^{-1}. Transducer signals for load and displacement were captured by a desktop computer using a high-speed data acquisition board and LabView software. Cylindrical specimens with a length to diameter ratio of 1.6 were used in compliance with ASTM standards (E9-81) for measuring the response of high-strength materials at large plastic strains, and the interfaces between the specimens and the compression platens were lubricated in order to avoid barreling of the specimens.

3.2. The compression Kolsky bar

The compression Kolsky bar (or split-Hopkinson pressure bar) developed by Kolsky (1949) was used to attain strain rates of 10^2–6×10^3 s^{-1}. This device consists of two long metal bars, designed to remain elastic throughout the test, that sandwich a small cylindrical specimen (the reader is referred to Coates and Ramesh (1991) for a more detailed description of the specific experimental setup used here). One end of the "input" bar is impacted by a projectile and the resulting compressive pulse propagates down the input bar to the specimen. Several reverberations of the loading wave occur within the specimen; a transmitted pulse is sent into the "output" bar and a reflected pulse is sent back into the input bar. Both the reflected and the transmitted pulses are measured using strain gages placed on the output and input bars. Once a uniform stress state is attained, the strain gage signals can be used to obtain the history of the strain rate and of the stress within the homogeneously deforming specimen (Coates and Ramesh, 1991). The strain rate is integrated over time to obtain the strain. By correlating the stress and strain histories, a stress–strain curve at a high strain rate is obtained from each test. Specimen recovery in the Kolsky bar was attained using the recovery modification, developed by da Silva and Ramesh (1997). Note that the bar-specimen interfaces are sufficiently lubricated so as to avoid any barreling of the specimen.

3.3. High-strain-rate pressure–shear plate impact experiments

The high-strain-rate pressure–shear plate impact technique was used, in order to study the very high-strain-rate (5×10^4–$10^6\,s^{-1}$) response of both the unreinforced alloy and of the composite. This technique was developed specifically for the study of the shearing behavior of materials undergoing homogeneous shearing deformations at extremely high shear rates while under superimposed hydrostatic pressures. (A more detailed description of this technique is provided by Clifton and Klopp (1985), and a description of the specific implementation of the technique used here is provided by Yadav et al. (1995).)

The high-strain-rate pressure–shear plate impact experiment involves the impact of plates that are flat and parallel but inclined relative to their direction of approach (Fig. 3). The specimen used is a thin (~100 μm) plate carried on a hard elastic plate (the "flyer"); the flyer is carried on a projectile, which is launched down the barrel of a gas gun (with velocity V_0) towards a stationary "target" plate. At impact, plane longitudinal (compressive) and transverse (shear) waves are generated in the specimen and the target plate. These waves reverberate within the specimen, remaining loading waves as the impedance of the material of the flyer and target plates (made of Carpenter D-3 tool steel) is higher than that of the specimen material. Due to the finite compressibility of the specimen, the normal stress in the specimen attains an equilibrium value. Measurements of the normal and transverse particle velocities at the free surface of the target plate are made using laser interferometers (a transverse displacement interferometer or TDI and a normal velocity interferometer or NVI) off a diffraction grating that is photo-deposited onto the rear surface. The

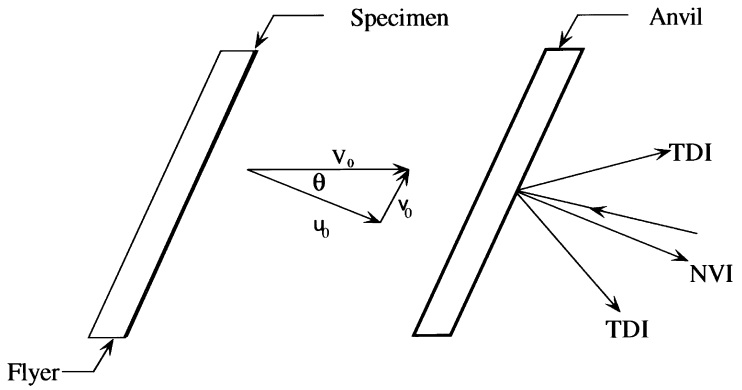

Fig. 3. Schematic configuration of the high-strain-rate pressure–shear plate impact experiment.

experiments are so designed that the target and flyer plates remain elastic, and hence the information on the stress levels sustained by the specimen material can be obtained by measuring particle velocities in the target plate. The entire experiment is completed before any unloading waves from the periphery of the plates arrive at the point of observation, so that only plane waves are involved and a one-dimensional analysis can be used. Such analysis of the interferometric data then provides a shear stress versus shear strain curve for the material under study at very high shear rates (on the order of 10^5 s^{-1}) and under superimposed compressive stresses (on the order of GPa).

3.4. Specimen preparation

The specimens for the quasistatic tests and Kolsky bar tests were cylinders (axis along the axis of the cast bar) with diameters of 5 mm and length/diameter ratios of 0.6 for the Kolsky bar experiments and 1.6 for the quasistatic experiments. Note that these aspect ratios are such that elastic information cannot be extracted from the data. The specimens were generated from the cast bar using electric discharge machining. A special jig was then used within a lapping machine so that the specimen ends were flat and parallel, and sufficient lubrication was used to avoid barreling of the specimens during the compression tests. The specimens for the pressure–shear plate impact tests were produced by first taking 400 μm thick transverse slices of the cast bar using an EDM, then coring the slices to generate circular plates with a diameter of 25.4 mm. Finally, these plates were lapped on both sides and reduced in thickness to around 150 μm for the A359 alloy specimens and to around 100–150 μm for the A359/SiC MMC specimens.

A note on the relevant length scales in pressure–shear plate impact experiments is in order, given the relatively coarse microstructure of the cast material. A fact that is not always appreciated is that although, the specimen thickness is only 100–150 μm, the actual length scale over which the pressure–shear test averages the properties is substantially larger, on the order of 20 mm in the plane. This is because of the nature of the test and the process of data acquisition. The shear stress as a function of time is measured at a point on the rear surface of the target plate or anvil. At any given time Δt after the beginning of shearing, information from an extended area of the anvil (with a radius given by $\sqrt{c_s \Delta t(c_s \Delta t + 2h)}$, where h is the anvil plate thickness and c_s is the shear wave speed in the anvil material) arrives at the point of measurement. For the typical time scales (0.5–1.0 μs) and the plate thicknesses of our experiments, this averaging occurs over more than two cm in the plane. The effective volume of material sampled is therefore substantial, and near bulk response is measured by the experiment even though the specimen thicknesses are small.

4. Experimental results

Experimental results will be presented for the unreinforced A359 alloy and the Alcan A359/SiC composite for mean strain rates of 10^{-4}, 10^{-2} and 1 s^{-1} using the servohydraulic machine, mean strain rates of 2×10^{3}–7×10^{3} s^{-1} using the compression Kolsky bar, and a nominal strain rate of 10^{5} s^{-1} using pressure–shear plate impact. For the tests at quasistatic rates, three specimens (5 mm in diameter and 8 mm long) were tested at each individual rate to achieve average representative data. For the Kolsky bar tests, five specimens (5 mm in diameter and 3 mm long) were tested at each individual rate. For the pressure–shear plate impact tests, two specimens were tested for each material at each rate.

A comparison of the true stress–strain curves obtained on the unreinforced A359 alloy and on the F3S.20S composite at the low strain rate of 10^{-4} s^{-1} is presented in Fig. 4. The increased flow strength of the composite, due to the presence of the reinforcing SiC particles is evident (note that the elastic response is not accurately measured because of the specimen aspect ratios). Once the substantial plastic flow has developed (after about 3% strain), the strain hardening of the composite is perceptibly smaller than that of its matrix alloy. Previous work, has shown that the strain hardening of MMC is normally similar to that of the corresponding matrix materials, and so the difference in strain hardening in this case suggests that some type of damage is developing within the composite, even during these compressive deformations. The quantitative determination of the evolution of the damage in the composite is a much more complex issue, and will be addressed in a separate article.

A summary of the rate-dependent mechanical response of the unreinforced A359 alloy is presented in Fig. 5 for a wide range of strain rates (from 10^{-4} to 2×10^{5} s^{-1}). The strength of the matrix material clearly increases substantially with strain rate, especially at the very high strain rates developed within pressure–shear plate impact. The plate impact results in Fig. 5 were converted from shear stress–shear strain data to true stress–true strain data using J_2-flow theory, which is thought to be a reasonable assumption for this aluminum alloy. The oscillations in one of the stress–strain curves from the plate impact are a result of poor signal-to-noise ratio and do not represent material behavior. Note that the degree of strain hardening of the

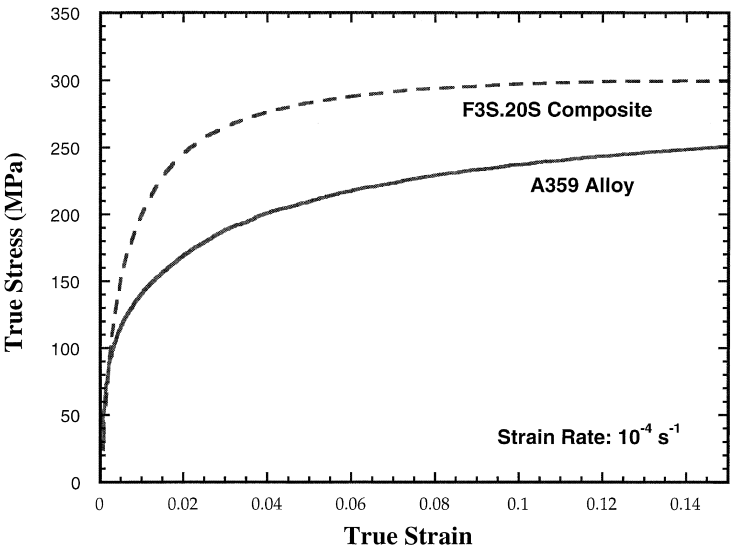

Fig. 4. Quasistatic response (strain rate of 10^{-4} s^{-1}) of the unreinforced A359 aluminum alloy and of the MMC. Note the strengthening effect of the reinforcement as well as the lower strain hardening evinced by the composite.

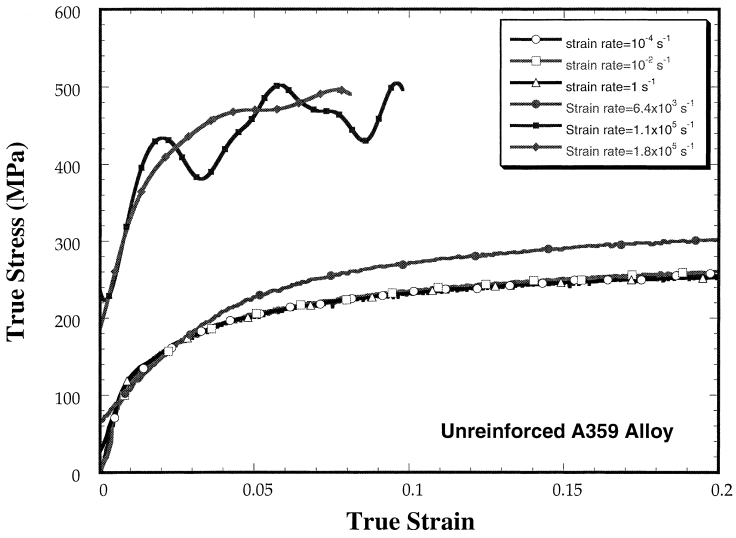

Fig. 5. Stress–strain curves obtained on the unreinforced A359 alloy over the full range of strain rates (pressure–shear data incorporated using the J_2-flow approach).

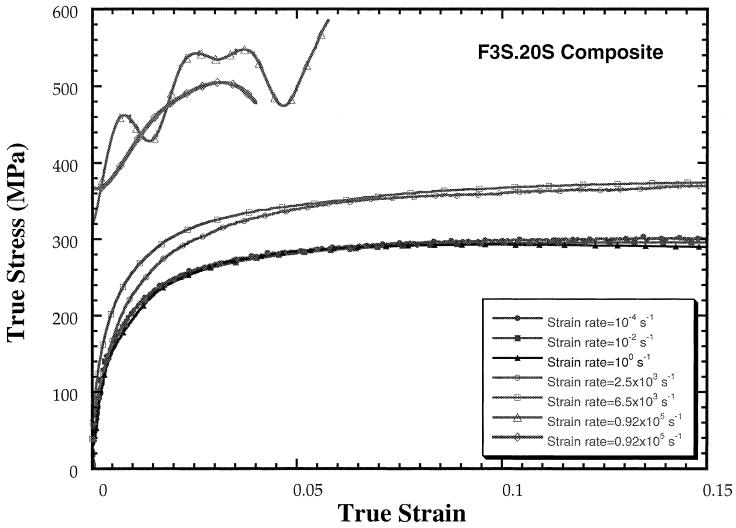

Fig. 6. Stress–strain curves obtained on the MMC (A359 alloy containing 20 vol% SiC particles) over the full range of strain rates; pressure–shear data again incorporated using the J_2-flow approach.

unreinforced material does not change significantly with strain rate (a slight reduction in hardening is expected at high rates because of the near-adiabatic nature of the high-rate experiments).

A similar set of results for the rate-dependent mechanical response of the F3S.20S MMC are presented in Fig. 6 for a similar range of strain rates (from 10^{-4} to 0.9×10^{5} s^{-1}). The composite also displays a substantial rate sensitivity, while consistently developing flow stresses higher than those sustained by the unreinforced alloy at the same strain rates and strains. A comparison of Figs. 5 and 6 indicates that the

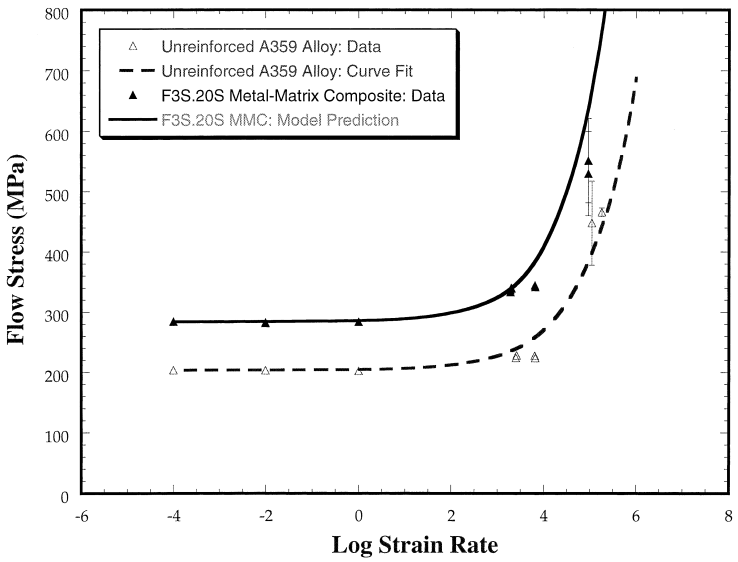

Fig. 7. Rate dependence of the flow stress for both the unreinforced A359 alloy and for the MMC, including data from pressure–shear plate impact using the J_2-flow approach. The rate dependence of the composite predicted by the model is also shown, as is the curve-fit to the matrix data used as input to the model.

reduction in strain hardening in the composite generally persists at high rates (although this is not clear for the plate impact results). Once again, the plate impact results were converted to the variables of Fig. 6 using J_2-flow theory. This is now a more questionable assumption, since information on the multi-axial response of MMCs is lacking at this time, and especially, since this particular composite appears to develop damage during compressive deformations. With this caveat, however, the response of the composite appears to be consistent with what one might expect, given the rate-sensitive properties of the matrix (Yadav et al., 1995).

The rate dependence of the stress–strain response of the composite and the unreinforced alloy can be conveniently compared within the rate-sensitivity diagram of Fig. 7, which plots the flow stress sustained by each material at a total strain of 5% as a function of the logarithm of the strain rate. It is apparent that the flow strength increases substantially at high strain rates for both the composite and the monolithic alloy, and the flow strength of the composite appears to increase as much as or slightly more than that of the unreinforced material. This observation is consistent with the experimental results reported by Perng et al. (1993a,b) and Yadav et al. (1995), and with the numerical results of Bao and Lin (1996) and Li and Ramesh (1998). Section 5 attempts to use the modeling approach of the latter paper to predict the observed response of our composite in terms of the known response of the matrix metal.

5. Numerical and analytical modeling

In a previous article, Li and Ramesh (1998) developed an analytical model (motivated by numerical results) for the high-strain-rate deformation of MMCs, and this model is applied to this specific composite in this section. The numerical results were obtained using axisymmetric unit cell models, with the particles treated as elastic ellipsoids or cylinders embedded within a viscoplastic matrix. The constitutive behavior of the matrix material assumed a power law strain-rate hardening formulation, with the parameters obtained from independent experimental results on the matrix. The flow stress of MMCs was then predicted over a

range of strain rates for different particle volume fractions and for varying particle shapes and particle aspect ratios. These results showed that both the flow stress and the strain rate hardening increased with increasing volume fraction of the reinforcement, and that the rate-dependent flow stress is influenced not only by particle aspect ratio but also by particle shape (spheroidal or cylindrical).

The microstructure of the composite, represented by Figs. 1(b) and 2, indicate that the reinforcing particles should be modeled as cylindrical (rather than spherical) inclusions, so as to account for the angularity of the particle corners (Song et al., 1996). The SiC particles are assumed to undergo only elastic deformations, with a Young's modulus of 450 GPa and a Poisson's ratio of 0.17. The aluminum alloy matrix is characterized as an isotropically hardening rate-dependent elastic–plastic solid that deforms elastically or elasto-plastically depending on the local effective stress level, with the properties determined from those of the unreinforced A359 aluminum alloy. The Young's modulus and Poisson's ratio of the matrix material are 69 GPa and 0.33, respectively; the onset of yielding is at an effective stress of 132 MPa. The assumed nonlinear stress–strain behavior of the matrix at lower strain rates is based on the experimental measurements (Fig. 4) of the A359 aluminum alloy at a rate of 10^{-4} s^{-1}. The experimental results on the unreinforced alloy were only obtained for strains less than 20%; for strains greater than 20%, it is assumed that the strain hardening rate remains the same as that between strains of 0.15 and 0.2 (i.e., the stress–strain curve at large strain is obtained by linearly extending that below 20%). The strain-rate hardening of the matrix is assumed to follow a power law:

$$\frac{\sigma}{\sigma_0} = 1 + \left(\frac{\dot{\varepsilon}^p}{\dot{\varepsilon}_0}\right)^m, \tag{1}$$

where σ_0 and $\dot{\varepsilon}_0$ are a reference stress and reference strain rate, respectively, with the parameters determined from the experimental data presented in Fig. 7. The parameters σ_0 and $\dot{\varepsilon}_0$ are taken as 241 MPa and 1.47×10^5 s^{-1}, respectively, while m is assumed to be 0.45. This choice of parameters provides an excellent fit to the rate-dependent flow stress of the matrix alloy, as shown by the curve in Fig. 7. Note that the availability of the plate impact data is useful for an accurate evaluation of the power m.

Given this complete characterization of the mechanical behavior of the matrix material, the numerical and analytical results of Li and Ramesh (1998) can be used to predict the rate-dependent response of the composite material (as the volume fraction of the particles, the particle shape, and particle aspect ratio are known). The analytical model for the rate-dependent response of the composite is represented by:

$$\sigma\left(f,\varepsilon,\dot{\varepsilon}\right) = \sigma_0(\varepsilon)g(f)\left(1+\left(\frac{\dot{\varepsilon}}{\dot{\varepsilon}_0}\right)^m\right)\left(1+\left(\frac{\dot{\varepsilon}}{\dot{\varepsilon}_0}\right)^m f\right), \tag{2}$$

where $\sigma_0(\varepsilon)$represents the stress–strain response of the matrix at quasistatic rates of deformation and is obtained directly from experiment (Fig. 4), $g(f)$ represents the variation of the flow stress ratio with the volume fraction f at quasistatic rates of deformation and is obtained from numerical calculations using unit cell models, and m and $\dot{\varepsilon}_0$ are the parameters previously discussed that determine the rate sensitivity of the matrix material. The work hardening of the matrix is incorporated within $\sigma_0(\varepsilon)$ and is assumed to be independent of the strain rate (a good assumption for the unreinforced A359 matrix alloy, vide Fig. 5). The last term in Eq. (2) represents the direct coupling of the strain-rate and the volume fraction effects. The strengthening function $g(f)$ must be evaluated numerically, as in Li and Ramesh (1998), for the specific particle shape and aspect ratio present in the composite. Fig. 2, indicates that the most common aspect ratios, 1.5 are in both the axial and transverse sections; however, the orientations of the particles (not shown in Fig. 2) are essentially random. As a result, the use of an aspect ratio of 1 in the model appears reasonable (because the model is based on axisymmetric unit cells, the introduction of nonunity aspect ratios necessarily introduces anisotropy into the results). The influence of aspect ratio has been shown

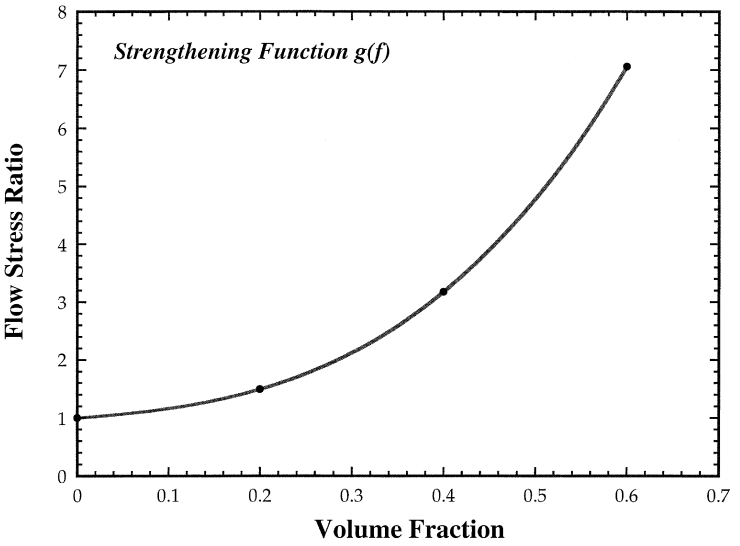

Fig. 8. Strengthening function $g(f)$ computed for this case using the axisymmetric unit cell model (elastic cylindrical particle of unit aspect ratio, matrix properties given by those of the unreinforced A359 alloy). The flow stress ratio is the ratio of the composite flow stress to the matrix flow stress.

(Li and Ramesh, 1998) to be dependent on the strain rate (i.e., the rate dependence and the aspect ratio dependence are coupled), but for near-unit aspect ratios the effect of the coupling is negligible, and so the form of model (2) remains reasonable. The form of the strengthening function $g(f)$ is typically that of a polynomial in the volume fraction f with the coefficients determined from the computations. Such axisymmetric cell computations have been performed for the specific matrix alloy considered here, and the resultant strengthening function is shown in Fig. 8. For the specific shape and aspect ratio used here, the function can be approximated as:

$$g(f) = 1 + 1.17f + 2.28f^2 + 21.0f^3. \tag{3}$$

As this article deals with a single MMC with a fixed particle volume fraction, the strengthening function in fact reduces to a single number that represents the strengthening effect of the particles at quasistatic rates of deformation. However, this modeling approach allows one to compute the effective responses for various volume fractions, an ability that is key to the successful design of graded armor structures. We note that this modeling approach, while being well established in the literature, involves several inherent approximations (discussed in the article by Li and Ramesh, 1998) that must be checked before applying the results directly to a wide range of composites.

6. Comparison of model with experimental results

The stress–strain curves predicted by the model are compared in Fig. 9 with the experimental measurements of the composite response at various strain rates. While the observed flow stresses are reasonably well predicted at small strains for strain rates less than 10^5 s^{-1}, the predicted flow stress increasingly overestimates the experimental flow stresses as the strain increases. That is, the model does an acceptable job of capturing the rate dependence of the composite but does not correctly capture the strain hardening of the composite. Because of the nature of the model and the assumed physics of large deformations, the

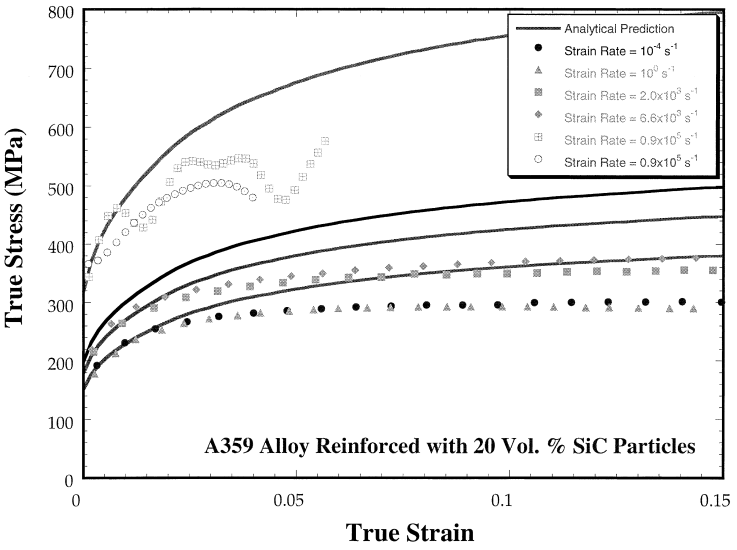

Fig. 9. Comparison of predicted and observed stress–strain curves for the composite over the full range of strain rates.

model predicts a strain hardening at large strains that is essentially the same as that of the matrix. Such an approach, has been shown (Li and Ramesh, 1998) to work well for a 6061-T6/Al_2O_3 composite (Yadav and Ramesh, 1995) and an 8090/SiC composite (Vaidya and Zurek, 1994). However, the experimental data (Figs. 5 and 6) also shows that the strain hardening of this A359-based composite material is significantly lower than that of the matrix material, which was not the case in the 6061-T6 and 8090 composites. It must be concluded, that there is something fundamentally different about the deformation mechanisms within the A359 composite (F3S.20S) investigated here. Indeed, microstructural examination of the deformed composite (Fig. 10) shows that substantial particle damage occurs within the F3S.20S composite even during these compressive deformations, whereas no damage of the particles was observed during the compression of the 6061-T6 and 8090 composites. The effect of this particle damage is to lower the flow

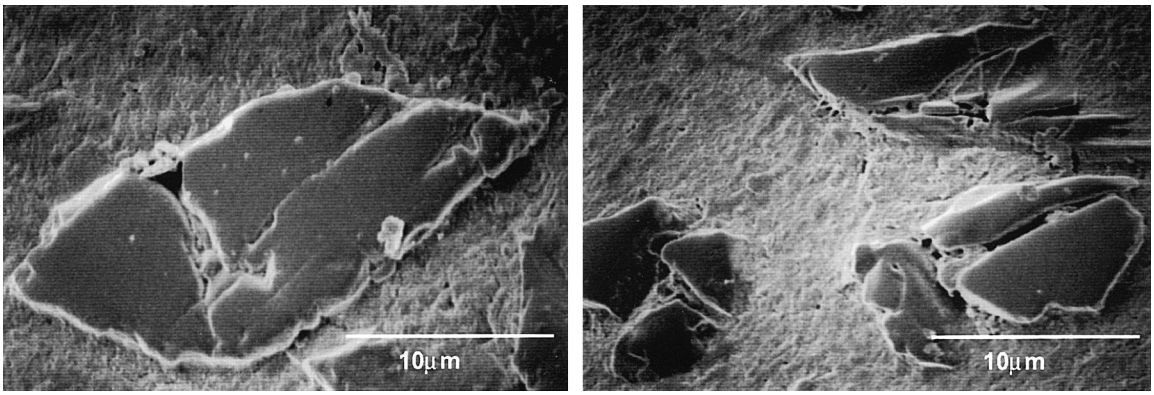

Fig. 10. Optical micrograph showing typical particle damage after quasistatic compressive deformations.

stress. As the model developed by Li and Ramesh (1998) does not account for damage, the model overestimates the composite flow stress.

It is also possible, that the discrepancy between the model and the experiment is a result of the debonding between the reinforcement and the matrix. While we do not have incontrovertible evidence that debonding does not occur within the F3S.20S composite, there is ancillary evidence that suggests that this is not a significant issue for the deformations considered here. In addition, to the fact that these deformations are compressive, some degree of debonding has been observed in the 6061-T6 and 8090 composites previously discussed, and yet the model predictions (which assume perfect bonding) are able to capture the observed behavior, suggesting that the effect of the typical degree of debonding on the composite flow stress in compression is small. It appears, therefore, that particle damage (particle fracture) is the dominant damage mode causing a reduction in the overall strain hardening of the composite material. This particle damage may be expected to accumulate with increasing strain in a manner similar to that suggested by many investigators for tensile tests (Lloyd, 1991). An improved model for this F3S.20S composite should therefore incorporate the effect of damage.

Fig. 7 also presents a comparison of the observed rate dependence of the composite response with the predicted rate dependence using Eq. (2). The dashed curve that passes through the matrix data represents one of the inputs to the model, whereas the solid curve that passes through the composite data points represents the output of the model (evaluated at a fixed strain of 5%). As the strain hardening is not correctly captured, the quality of the prediction of the composite response will be progressively worse as increasing strains are considered. For small strains, however, and for strain rates up to 10^3 s^{-1}, the model provides a fairly good approximation to reality.

Figs. 7 and 9 both show that the flow stresses predicted by this model at a strain rate of 10^5 s^{-1} are significantly higher than the flow stresses observed in the pressure–shear plate impact experiments. Some of this discrepancy is likely because the experiment is nearly adiabatic while the model is essentially athermal, but we believe this contribution to be small for these particular experiments because the temperature rise is small. Further, the input matrix high-rate data for the models is also affected by thermal softening at high rates, so some thermal softening is implicitly incorporated through the rate dependence parameters. A more significant contribution likely arises from the multi-axial nature of the deformations developed in such experiments: the pressure–shear plate impact technique provides shear stress vs. shear strain data, and the corresponding overall flow stress in uniaxial compression is obtained assuming J_2-flow theory for the purposes of Figs. 6 and 8. Because of the presence of the particles and the probable progressive damage developed within the particles, this assumption may well be in error, accounting for some of the discrepancy.

7. Discussion

The experimental results presented here represent the first full viscoplastic characterization of a cast aluminum alloy. Such a characterization is useful because a number of recent manufacturing approaches are making use of cast alloys, and the viscoplastic properties are necessary for appropriate design. The results on the A359 aluminum alloy are also interesting from a materials viewpoint, in that the microstructures of the cast alloys are generally very different from the microstructures of the wrought alloys. The data presented here indicate that the viscoplastic response of the cast A359 aluminum alloy is very similar in a number of ways to the viscoplastic response (Yadav et al., 1995) of the wrought 6061 aluminum alloy (in the peak-aged condition), with substantial rate sensitivity at high strain rates and with a strain hardening that is insensitive to strain rate (an FCC characteristic). It is also clear, however, that the A359 aluminum alloy is significantly weaker than the 6061-T6 aluminum alloy, and that the as-cast material has a stronger strain hardening response than the wrought aluminum alloy.

The primary interest in the viscoplastic response of the F3S.20S composite material derives from the potential applications of such composites within graded armor structures. Graded armor structures based on cast aluminum alloy matrices have the advantage of greatly reduced manufacturing cost in comparison to the costs of FGM processing by powder metallurgy routes. Simultaneously, these materials provide improved ballistics at lower weight than conventional armor (weight and cost reductions are major drivers within advanced armor initiatives). Prediction of the ballistic performance and design of graded and layered armor structures requires knowledge of the viscoplastic response of such MMCs as a function of ceramic volume fraction. The experiments and modeling presented here provide the first steps in that direction. These results clearly indicate, that there is much strength to be gained at high strain rates by changing the ceramic volume fraction. Other variables such as particle size, shape, aspect ratio, and distribution are certainly also of great interest. Earlier work by the authors (Li and Ramesh, 1998) has examined the shape and aspect ratio effects on the viscoplastic response, and work on the size effect is in progress. The experimental results presented here are unique in that they include data at strain rates of nearly 10^5 s^{-1}.

The observation that particle damage develops within this composite during purely compressive deformations at all strain rates is consistent with previous work on this material at low strain rates and various temperatures by Barnes et al. (1995). It should be pointed out that the SiC particles are polycrystalline (with an average grain size of 3–5 μm) in this composite. As the SiC is very susceptible to intergranular cracking, the particles are broken into several pieces along the grain boundaries. Such damage phenomena are of great importance in ballistic problems, where initial compression is often followed by local tension. Compressive damage has not been observed in several other MMCs, even at high strain rates. It would appear that a combination of effects including matrix behavior, particle shape, CTE mismatch, interface characteristics and low ceramic fracture toughness play a part in the evolving damage phenomenon; a subsequent article addressing this issue is under preparation.

Residual stresses arise from the thermal expansion mismatch between the ceramic particles and metal matrix as a result of thermomechanical processing. However, Taggart and Bassani (1991) performed a systematic analysis of the effect of residual stresses on the elastic–plastic behavior of particle-reinforced composites, and concluded that the enhanced hardening, due to residual stresses, diminishes as the strain becomes large. That is, at large plastic strains, the effects of the residual stresses are relatively small. Thus, residual stress effects do not significantly affect the results, presented in the current article, which are primarily obtained at relatively large plastic strains.

8. Summary

The mechanical behavior of an A359/SiC_p MMC and of the corresponding A359 matrix alloy has been measured in compression over a wide range of strain rates (10^{-4}–10^5 s^{-1}) using several different experimental techniques. The results show that:

1. Both the A359 matrix alloy and the A359/SiC_p composite show rate dependence of the flow stress in compression, with rate dependencies that increase with increasing strain rate.
2. The unreinforced A359 alloy shows strain hardening that is essentially independent of the strain rate, similar to observations made on FCC metals.
3. The A359/SiC_p composite shows significantly less strain hardening than does the corresponding matrix alloy. This reduction in strain hardening appears to be a result of the progressive particle fracture during these compressive deformations.
4. The model developed by Li and Ramesh (1998) is able to capture the rate dependence of the flow stress of the composite, and is able to provide a reasonable estimate of the flow stress of the composite material at small strains. However, because the model does not incorporate the particle damage that occurs in

the composite, it is unable to predict the changed overall strain hardening of the composite material. A model incorporating the effect of damage will be presented in a forthcoming article.

Acknowledgements

This work was supported by the US Army Research Office under Grant No. DAAH04-95-2-0006 and by the US Army Research Laboratory through Grant No. DAAL01-96-2-0047. The authors wish to express appreciation for the assistance of A.M. Lennon and D. Jia with the experiments. Last but not the least, the authors would like to thank Don Doutre of Alcan International Ltd. for supplying them with both the unreinforced alloy and the composite material.

References

Bao, G., Lin, Z., 1996. High strain rate deformation in particle reinforced metal matrix composites. Acta Mater. 44 (3), 1011–1019.

Barnes, S.J., Prangnell, P.B., Roberts, S.M., Withers, P.J., 1995. The influence of temperature on microstructural damage during uniaxial compression of aluminium matrix composites. Scripta Metall. et Mater. 33 (2), 323–329.

Chichili, D.R., Ramesh, K.T., 1995. Dynamic failure mechanisms in a 6061-T6 Al/Al_2O_3 metal–matrix composite. Int. J. Solids Structr. 32 (17/18), 2609–2626.

Christman, T., Needleman, A., Nutt, S., Suresh, S., 1989a. On microstructural evolution and micromechanical modeling of deformation of a whisker-reinforced metal–matrix composite. Mat. Sci. Engng. A 107, 49–61.

Christman, T., Needleman, A., Suresh, S., 1989b. An experimental and numerical study of deformation in metal–ceramic composites. Acta Metall. 37 (11), 3029–3050.

Clegg, W.J., 1988. A stress analysis of the tensile deformation of metal–matrix composites. Acta Metall. 36 (8), 2141–2149.

Clifton, R.J., Klopp, R.W., 1985. Pressure–shear plate impact testing. In: American Society of Metals Handbook, vol. 8. ASM International, pp. 230–239.

Coates, R.S., Ramesh, K.T., 1991. The rate-dependent deformation of a tungsten heavy alloy. Mat. Sci. Engng. A 145, 159–166.

da Silva, M., Ramesh, K.T., 1997. The rate-dependent deformations of porous pure iron. Int. J. Plast. 13 (6/7), 587–610.

Gray III, G.T., Hixson, R.S., Johnson, J.N., 1996. Dynamic deformation and fracture response of a 6061-T6 Al – 50 vol% Al_2O_3 continuous reinforced composite. In: Schmidt, S.C., Tao, W.C. (Eds.), Shock Compression of Condensed Matter 1995, American Institute of Physics, Woodbury, New York, pp. 547–550.

Guden, M., Hall, I.W., 1998. Dynamic properties of metal matrix composites: a comparative study. Mat. Sci. Engng. A 242, 141–152.

Harding, J., Derby, B., Pickard, S.M., Taya, M., 1987. An investigation of the high-rate deformation of SiCw/2124 Al composite. In: Matthews, F.L. et al. (Eds.), Proc. Sixth Int. Conf. on Composite Materials (ICCM VI), vol. 3, Elsevier, London, pp. 76–85.

Hong, S.I., Gray III, G.T., 1994. Dynamic mechanical response of a 1060 Al/Al_2O_3 composite. J. Mater. Sci. 29, 2987–2992.

Kolsky, H., 1949. An investigation of the mechanical properties of materials at very high rates of loading. Proc. the Physical Society, London 62B, p. 676.

Li, Y.L., Ramesh, K.T., 1998. Influence of particle volume fraction, shape and aspect ratio on the behavior of particle-reinforced metal–matrix composites at high rates of strain. Acta Mater. 46 (16), 5633–5646.

Lloyd, D.J., 1991. Aspects of fracture in particulate reinforced metal matrix composites. Acta Metall. Mater. 39 (1), 59–71.

Marchand, A., Duffy, J., Christman, T.A., Suresh, S., 1988. An experimental study of the dynamic mechanical properties of an Al–SiCw composite. Engng. Frac. Mech. 30, 295–315.

Mortensen, A., Suresh, S., 1995. Functionally graded metals and metal–ceramic composites: part 1 processing. Int. Mat. Rev. 40 (6), 239.

Mukai, T., Nieh, T.G., Higashi, K., 1995. Influence of strain rate on the mechanical properties in a magnesium-base composite. In: Murr, L.E., Staudhammer, K.P., Meyers, M.A. (Eds.), Metallurgical and Materials Applications of Shock-Wave and High-Strain-Rate Phenomena, Elsevier, Amsterdam, pp. 885–891.

Perng, C.C., Hwang, J.R., Doong, J.L., 1993a. High strain rate tensile properties of an (Al_2O_3 particles)-(6061-T6 Al alloy) metal–matrix composite. Mat. Sci. Engng. A 171, 213–221.

Perng, C.-C., Hwang, J.-R., Doong, J.-L., 1993b. The effect of strain rate on the tensile properties of an Al_2O_3/6061-T6 aluminum metal–matrix composite at low temperatures. Scripta Metall. et Mater. 29, 311–316.

Song, S.G., Shi, N., Gray III, G.T., Roberts, J.A., 1996. Reinforcement shape effects on the fracture behavior and ductility of particular-reinforced 6061-Al matrix composites. Metall. Mat. Trans. 27A, 3739–3746.

Suresh, S., Mortensen, A., 1997. Functional graded metals and metal–ceramic composites: part 2 thermomechanical behavior. Int. Mat. Rev. 42 (3), 85.

Taggart, D.G., Bassani, J.L., 1991. Elastic–plastic behavior of particle reinforced composites – influence of residual stresses. Mech. Mat. 12, 63–80.

Taya, M., Mori, T., 1987. Dislocations punched-out around a short fiber in a short fiber metal matrix composite subjected to uniform temperature change. Acta Metall. 35 (1), 155–162.

Tvergaard, V., 1990. Analysis of tensile properties for a whisker reinforced metal–matrix composite. Acta Metall. et Mater. 38 (2), 185–194.

Vaidya, R.U., Song, S.G., Zurek, A.K., Gray III, G.T., 1996. The effect of structural defects in SiC particles on the static and dynamic mechanical response of a 15 volume percent SiC/6061-Al matrix composite. In: Schmidt, S.C., Tao, W.C. (Eds.), Shock Compression of Condensed Matter, American Institute of Physics, Woodbury, New York, 1995, pp. 643–646.

Vaidya, R.U., Zurek, A.K., 1994. Dynamic mechanical deformation of a SiCp/Al–Li (8090) composite. In: Schmidt, S.C. et al. (Eds.), High Pressure Science and Technology, American Institute of Physics, New York, 1993, pp. 773–776.

Yadav, S., 1996. An Experimental and Numerical Investigation of Dynamic Deformations in Metal–Matrix and Tungsten-Based Composites, Ph.D. Dissertation, The Johns Hopkins University.

Yadav, S., Chichili, D.R., Ramesh, K.T., 1995. The mechanical response of a 6061-T6 Al/Al_2O_3 metal matrix composite at high rates of deformation. Acta Metall. Mater. 43 (12), 4453–4464.

Yadav, S., Ramesh, K.T., 1995. The mechanical properties of tungsten-based composites at very high strain rates. Mat. Sci. Engng. A 203, 140–153.